doi:10.1016/j.jmb.2004.08.009 J. Mol. Biol. (2004) 342, 1625–1636

JMB

Available online at www.sciencedirect.com

SCIENCE DIRECT®

ELSEVIER

The Disintegrin Echistatin Stabilizes Integrin αIIbβ3's Open Conformation and Promotes Its Oligomerization

Roy R. Hantgan[1]*, Mary C. Stahle[1], John H. Connor[1], Douglas S. Lyles[1] David A. Horita[1], Mattia Rocco[2], Chandrasekaran Nagaswami[3] John W. Weisel[3] and Mary Ann McLane[4]

[1]*Department of Biochemistry Wake Forest University School of Medicine, Winston-Salem NC 27517, USA*

[2]*Medicina Rigenerativa, Istituto Nazionale per la Ricerca sul Cancro, Genova I-16132, Italy*

[3]*Deparment of Cell and Developmental Biology University of Pennsylvania Philadelphia, PA 19104, USA*

[4]*Department of Medical Technology, University of Delaware, Newark, DE 19716 USA*

**Corresponding author*

We have employed echistatin, a 5.4 kDa snake venom disintegrin, as a model protein to investigate the paradox that small ligand-mimetics can bind to the resting αIIbβ3 integrin while adhesive macromolecules cannot. We characterized the interactions between purified human αIIbβ3 and two recombinant echistatin variants: rEch (1-49) M28L, chosen for its selectivity toward β3-integrins, and rEch (1-40) M28L, a carboxy-terminal truncation mutant. While both contain an RGD integrin targeting sequence, only rEch (1-49) M28L was an effective inhibitor of αIIbβ3 function. Electron microscopy of rotary shadowed specimens yielded a variety of αIIbβ3 conformers ranging from compact, spherical particles (maximum dimension 22 nm) to the classical "head with two tails" forms (32 nm). The population of larger particles (42–56 nm) increased from 17% to 28% in the presence of rEch (1-49) M28L, indicative of ligand-induced oligomerization. Sedimentation velocity measurements demonstrated that both full length and truncated echistatin perturbed αIIbβ3's solution structure, yielding slower-sedimenting open conformers. Dynamic light scattering showed that rEch (1-49) M28L protected αIIbβ3 from thermal aggregation, raising its transition mid-point from 46 °C to 69 °C; a smaller shift resulted with rEch (1-40) M28L. Sedimentation equilibrium demonstrated that both echistatin ligands induced substantial αIIbβ3 dimerization. van't Hoff analysis revealed a pattern of entropy/enthalpy compensation similar to tirofiban, a small RGD ligand-mimetic that binds tightly to αIIbβ3, but yields smaller conformational perturbations than echistatin. We propose that echistatin may serve as a paradigm for understanding multidomain adhesive macromolecules because its ability to modulate αIIbβ3's structure resides on an RGD loop, while full disintegrin activity requires an auxiliary site that includes the carboxy-terminal nine amino acid residues.

Keywords: integrin; disintegrin; conformation; oligomerization; thermodynamics

Introduction

Integrin regulation of cellular adhesiveness is central to physiological processes ranging from embryonic development to programmed cell death, and aberrant integrin activation contributes to thrombosis, cancer and inflammatory disorders.[1] However, the molecular mechanisms that convert resting integrins into dynamic receptors, capable of sensing and responding to changes in a cell's external environment, remain a matter of intense investigation and some controversy.[2–4] The controversy arises in part from the divergent views of the structural basis for integrin activation provided by X-ray diffraction crystallography,[5,6] electron microscopy,[7–10] and biophysical solution conformation probes.[10–13] Resolution of this dilemma has proven problematic because most studies describing integrin–ligand interactions have used constitutively active ectodomain constructs.[1,14,15] In a previous study, Weisel *et al*.[16] analyzed native αIIbβ3 integrins bound to fibrinogen; however,

Abbreviations used: GST, glutathione-*S*-transferase; PRP, platelet-rich plasma; GFP, gel-filtered platelets.

E-mail address of the corresponding author: rhantgan@wfubmc.edu

their study was not designed to elucidate the mechanisms for ligand-linked conformational changes. Thus, we have chosen to revisit this issue using echistatin as a model protein ligand.

The conventional view of integrin structure, based on electron microscopy images, showed integrins as elongated molecules with an oval head from which two tails extend.[7,17,18] This was challenged when the first high resolution structure of an integrin ectodomain was published in 2001.[5] Examination of the crystal structure of the extracellular domain of αvβ3 revealed a sharply bent, multidomain molecule whose V-shape was preserved even when an Arg-Gly-Asp ligand was diffused into the crystals.[5,6,19] While some have argued that crystal packing artifacts limited the range of ligand-linked structural rearrangements,[20] Xiong *et al*.[2] have proposed a "deadbolt" model where reversible inter-domain contacts within the bent conformer regulate αvβ3 binding function. Small angle X-ray scattering data recently reported by Mould *et al*.[21] on an α5β1 ectodomain construct demonstrated that no large integrin conformational changes took place upon binding a fibronectin fragment (Fn 6-10). The combination of X-ray diffraction and X-ray scattering data would seem to indicate that integrin activation or "priming"[3] does not require large conformational changes, but this concept is not universally accepted.

In contrast to the minimalist view, Takagi & Springer have proposed a "switchblade" mechanism of integrin activation[22] based on electron microscopy and biophysical data, as well as mutationally engineered structural constraints and perturbations.[8,23–25] Takagi *et al*.[26] also presented electron microscopy images of an α5β1 ectodomain: fibronectin fragment (Fn 7-10) complex with a pronounced separation in the integrin's remnant stalks. Evidence that these ectodomain conformational changes may propagate across the plasma membrane to an integrin's cytoplasmic regions comes from *in vivo* FRET measurements that show a >100 Å cytodomain separation on αLβ2 integrin-cyan (or yellow) fluorescent protein constructs, activated by either inside–out or outside–in signaling.[27]

Both the deadbolt and switchblade models provide an attractive mechanism to explain integrin activation, but a note of caution is in order because the barriers that prevent resting, full-length integrins from binding macromolecular ligands have yet to be fully elucidated. For example, Adair & Yeager[9] used electron cryo-microscopy to obtain a 20 Å resolution structure for the intact αIIbβ3 complex, isolated and imaged in octyl glucoside micelles. The resulting model of the ligand-free integrin exhibited a large ectodomain connected by a narrow rod-like putative transmembrane domain to a small bilobed segment, assigned to the αIIbβ3 cytodomains. Their model was more compact than the extended integrins typically observed by TEM,[7,10,12] yet its ectodomain appeared less severely bent than the αvβ3 crystal structure.[5] Concerning integrin–ligand interactions, Adair & Yeager also reported electrophoretic mobility data indicating that echistatin, a 5.4 kDa RGD-containing disintegrin polypeptide found in *Echis carinatus* venom,[28–31] induced a transition in αIIbβ3 from a low to a high-affinity state.[9] However, they did not present any images of the integrin–echistatin complex.

We have also employed an integrated biophysical and electron microscopy approach to describe the links between ligand binding and integrin conformational changes.[10,12,13,32] Hence, we recognized in echistatin the opportunity to critically evaluate the mechanisms for integrin activation using both a full-length integrin and a protein ligand, rather than ligand-mimetics whose binding modes may not fully reflect the intricacies of αIIbβ3's interactions with its physiological binding partners. Echistatin is a model protein that presents both a paradox and a paradigm for understanding the regulation of integrin function. The paradox comes from the observation that echistatin binds with comparable affinity to αIIbβ3 complexes on both resting and stimulated human blood platelets,[33] whereas adhesive proteins such as fibronectin and fibrinogen display high-affinity interactions only with the "activated" receptor.[34] The paradigm derives from the common RGD–integrin targeting sequence shared by echistatin and αIIbβ3's primary physiological ligands.[35,36] In the experiments presented here, we will demonstrate that echistatin perturbs the resting receptor, and stabilizes an open conformer with an enhanced, entropy-driven oligomerization constant. We will show that echistatin's ability to modulate αIIbβ3's solution structure resides primarily within the RGD segment that protrudes from its disulfide-bonded core, while full disintegrin activity requires its carboxy-terminal segment.

Results

Recombinant echistatin variants and their biological activities

Echistatin is a member of the disintegrin family of low-molecular mass proteins that employ an Arg-Gly-Asp integrin targeting sequence to bind to and block integrin function.[37] A nearby methionine residue also contributes to echistatin's selectivity for certain integrins, as mutation to leucine disrupted binding to α5β1, but had no effect on binding to the β3 integrins.[38] In addition, echistatin has a putative auxiliary binding site at its carboxy terminus.[39,40] Thus, we examined the interactions of full-length (rEch (1-49) M28L) and truncated (rEch (1-40) M28L) recombinant echistatin variants[41] with the purified αIIbβ3 integrin, isolated in a functional conformation in octyl glucoside micelles.[10,11,13]

We assessed the ability of each recombinant echistatin variant to inhibit platelet aggregation and platelet adhesion to fibrin, two activities that

are dependent on the αIIbβ3 integrin.[32,42,43] rEch (1-49) M28L exhibited an $IC_{50}=126(\pm37)$ nM for inhibition of ADP-stimulated platelet aggregation, a parameter that agreed well with the values of 136(±29) nM and 124(±18) nM reported by Wierzbicka-Patynowski *et al*.[38] for native and recombinant echistatin (1-49), respectively. In contrast, rEch (1-40) M28L had no effect on platelet aggregation at concentrations ranging from 100 nM to 1000 nM. rEch (1-49) M28L also proved to be an effective inhibitor of platelet adhesion to clotted fibrin,[32] yielding $IC_{50}=124(\pm88)$ nM. Consideration of the platelet count and integrin receptor density[32] indicates that rEch (1-49) M28L caused a 50% reduction in platelet adhesive function at a four- to sixfold molar excess over its target, the αIIbβ3 integrin. In fact, the effectiveness of rEch (1-49) M28L in blocking platelet–fibrin interactions was comparable to the cyclic peptide integrin antagonists cHArGD and eptifibatide,[13] and exceeded that of the ligand-mimetic tirofiban.[32]

Effects of recombinant echistatin on αIIbβ3 structure examined by transmission electron microscopy

The effects of full-length echistatin on αIIbβ3 conformation and oligomerization were probed by examining rotary shadowed samples of the free and ligand-bound receptors by transmission electron microscopy. We observed a variety of αIIbβ3 conformers, in both the absence and presence of rEch (1-49) M28L, ranging from compact, spherical particles to the classical head with two tails forms.[7,10] Some of these particles appeared to have separate nodules corresponding to either a split in the head domain, as we reported earlier in the presence of ligand-mimetic peptides,[10,12] or separate stalks, as others have described.[8,27,44] Integrin dimers, joined through tail-to-tail contacts similar to those observed with αIIbβ3 and synthetic ligands,[10–13,32] or Mn^{2+},[44] were also present. Examples of the most common forms observed are illustrated in Figure 1; however, this image is not meant to represent the frequency of occurrence of these particles.

Given this multiplicity of integrin morphologies, we measured the distribution of particle sizes for both free and bound receptors, using the maximum linear dimension of each object as an index (SigmaScan; Jandel Scientific). As indicated in the histograph in Figure 1, comparable size distributions resulted for both free and bound integrins. The free αIIbβ3 complex exhibited a mean particle length of 30.7(±9.7) nm ($N=677$); 31.8(±9.7) nm ($N=622$) was obtained in the presence of rEch (1-49) M28L. While the difference between these mean particle sizes was small, it did achieve statistical significance ($p=0.02$, *t*-test[45]).

Further interpretation of these data was facilitated by comparing these parameters to models of the full-length αIIbβ3 complex in conformations ranging from bent,[5,9] to fully extended.[8,13,27] The surface representations of each model presented in Figure 1 were prepared, and their maximum linear dimensions calculated, using the molecular graphics package MolMol.[46] The experimentally determined mean particle dimensions (31–32 nm) correspond quite closely to the calculated parameters of 31 nm and 32 nm for the extended and stalk-split models, respectively. Modeling demonstrated that docking echistatin to αIIbβ3's ectodomain increased these calculated maximum particle lengths by ~1 nm, an observation that may also explain the experimentally determined distribution means for αIIbβ3 alone and in the presence of echistatin.

To explore this issue further, we fitted the experimental data obtained with αIIbβ3 alone to a sum of Gaussian distributions using an automated peak finding algorithm (PeakFit; Systat Software, Inc.). This procedure identified a major peak at 32 nm and smaller peaks at 20, 44 and 56 nm, as illustrated by the black lines in the histograph shown in Figure 1. (A minor peak at ~3 nm, most likely octyl glucoside micelles,[10] was omitted from the fitting procedure.) A similar pattern of peaks: 32, 22, 42, and 54 nm was detected in the presence of echistatin (gray lines). Systematically removing these peaks resulted in a two- to fourfold increase in the fit standard error, a goodness-of-fit parameter that accounts for changes in the degrees of freedom.[45] Therefore, we concluded that the four-peak fit best described the experimental data. Interestingly, the population tentatively identified as bent conformers (20–22 nm) was essentially unchanged in the presence (12%) or absence (13%) of echistatin, while the population of extended integrins (32 nm) decreased from 81% to 68% and the oligomer population (42–56 nm) increased from 17% to 28%. Interpretation of these data was aided by the models of tail-to-tail integrin oligomers (calculated length 50 nm) shown in Figure 1.

These observations suggest that echistatin promotes integrin oligomerization, so to clarify this issue, we also examined echistatin's effects on the αIIbβ3 solution conformation with three complementary biophysical techniques that we found to be sensitive indicators of tertiary and quaternary structural changes induced by synthetic integrin ligands: sedimentation velocity, dynamic light-scattering, and sedimentation equilibrium.[10–13,32]

Effects of recombinant echistatin variants on αIIbβ3 solution structure

We have previously demonstrated that ligand-mimetics that share with echistatin an RGD integrin-targeting sequence perturb the conformation of the purified αIIbβ3 integrin, yielding an "open" conformer with increased frictional drag.[10,32] Hence, we employed our most sensitive conformational probe, sedimentation velocity measurements coupled with time-derivative analyses,[47] to determine the effects of rEch (1-49) M28L and rEch (1-40) M28L on αIIbβ3 solution structure. As demonstrated in Figure 2(A), an equimolar

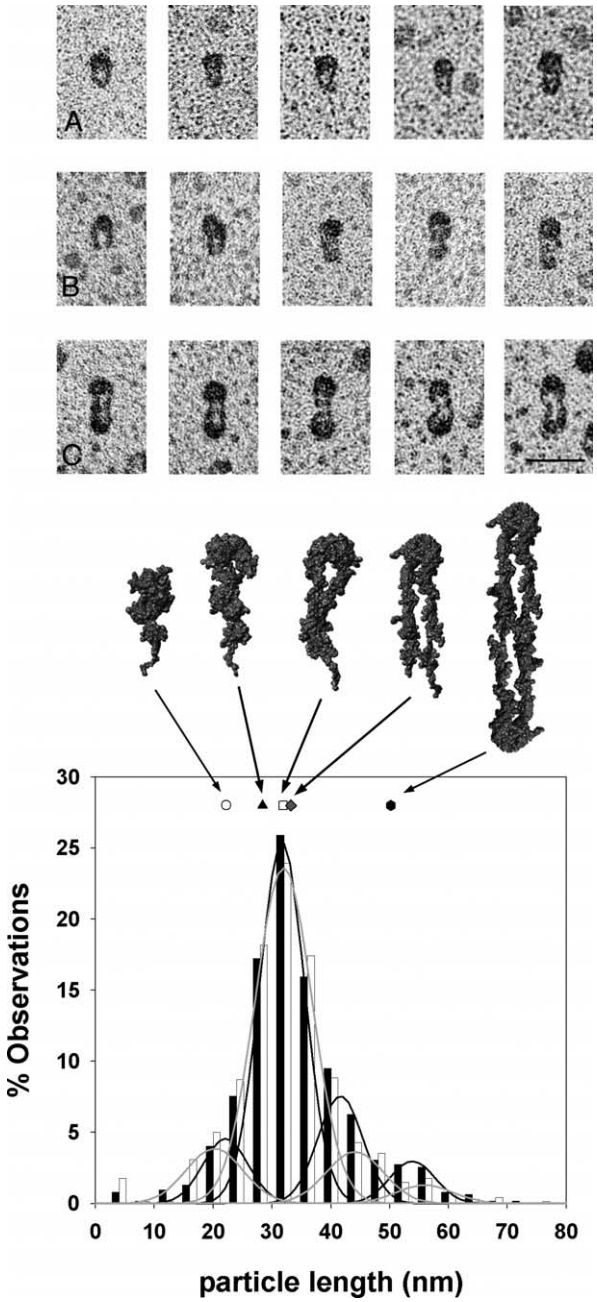

Figure 1. Transmission electron microscopy of rotary shadowed integrin in the presence and absence of echistatin; micrographs, models and measurements. Image gallery: (A) control integrin αIIbβ3, which consists of a globular head-piece and two tails, usually touching each other. In all experiments a variety of structures were observed, but only examples of the most commonly observed forms are shown here. (B) Integrin αIIbβ3 in the presence of echistatin. Again, a variety of structures were observed, but some examples of the most commonly observed forms are shown. Integrin complexes have the same general appearance as the controls but the total length of most molecules is slightly longer. (C) Examples of dimers of αIIbβ3 in the presence of echistatin. It is important to note that dimers are present in the control integrin and integrin with echistatin, but only a small fraction of integrins are present as dimers. Integrin models: the panel below shows models (and maximum dimensions) of the full-length αIIbβ3 complex, including bound octyl glucoside micelles, corresponding to the following structures: the αvβ3 ectodomain crystallographic structure (open circle),[5] the αIIbβ3 cryo-electron microscopy 3D model (filled triangle),[9] our extended αIIbβ3 model (open square),[13] and the cytoplasmic domain separation model (filled diamond) proposed by Springer and colleagues.[8,27] Our model of a tail-to-tail integrin dimer[13] is denoted by a filled circle. The calculated maximum dimensions of each of these models are indicated by the symbols at the top of the Figure below. Integrin dimensions: The histograph depicts the distribution of integrin particle sizes observed in the absence (open bars) or presence (filled bars) of recombinant echistatin. The continuous lines define the peaks detected by fitting the experimentally observed distributions to a sum of Gaussian peaks (Peak Fit, Systat Software, Inc.); the gray lines identify peaks in the control integrin samples and the black lines in the integrin–echistatin samples.

concentration of rEch (1-49) M28L shifted αIIbβ3's g(S) profile (open circles) toward a slower-sedimenting conformer (gray circles); comparable effects were observed at a tenfold molar excess (filled circles). The effects of the truncated echistatin were somewhat less pronounced when present at an equimolar concentration, but were similar to the full-length disintegrin at a tenfold molar excess (Figure 2(B)).

Preliminary hydrodynamic computations using the SOMO algorithms[48–50] indicate that a resting integrin–echistatin complex would exhibit a sedimentation coefficient ~2% larger than the ligand-free integrin. In contrast, computations based on models like those presented in Figure 1 indicate that ligand-induced structural asymmetry would decrease the receptor's sedimentation coefficient by some 4–12%. As illustrated by the symbols at the top of Figure 2(A), $S_{\text{bent}} > S_{\text{partially extended}} > S_{\text{fully extended/echistatin}} > S_{\text{stalk split/echistatin}}$. Thus, the experimentally determined decreases in S are most likely due to conformational changes in the receptor linked to echistatin binding.

Examination of a range of echistatin concentrations demonstrated a 7.2($\pm$1.3)% decrease in αIIbβ3's sedimentation coefficient for rEch (1–49) M28L and a comparable 5.5($\pm$1.8)% decrease for rEch (1–40) M28L (Figure 2(C)). These data indicate that echistatin's 11 residue carboxy-terminal segment is not required for the ligand to perturb αIIbβ3's solution conformation. Consideration of the complete data set demonstrated that the effects of both rEch (1-49) M28L and rEch (1-40) M28L on αIIbβ3's sedimentation profile were statistically significant ($p < 3 \times 10^{-3}$ in both cases; t-test[45]). The effects of rEch (1-49) M28L on αIIbβ3 conformation were not readily reversible, as removing excess ligand following a one hour incubation still yielded a slower-sedimenting conformer (Figure 2(C), open circle). These observations provide direct evidence that binding a single-domain protein ligand to a full-length integrin yields a species with a conformation distinct from that of the free receptor.

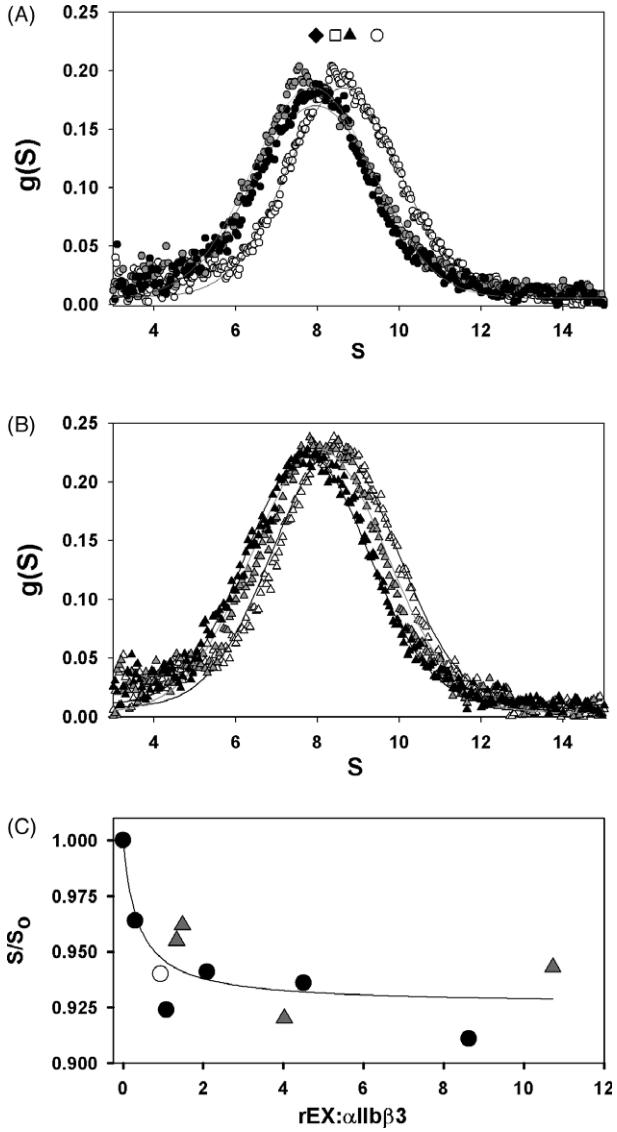

Figure 2. Effects of recombinant echistatin on αIIbβ3 solution conformation determined by sedimentation velocity. (A) Data obtained for αIIbβ3 alone (open circles), +rEch (1-49) M28L at an equimolar concentration of (gray circles), or a tenfold molar excess (filled circles) were analyzed with time-derivative software (DCDT+, J. Philo[77]) to obtain sedimentation coefficient distribution functions, $g(s^*)$ *versus* s^*.[47] Continuous lines were obtained by fitting the resultant distribution functions to a single ideal species. Top symbols denote the computed sedimentation coefficients for the models illustrated in Figure 1.[49,50] (B) Sedimentation velocity data obtained with αIIbβ3 alone (open triangles), +rEch (1-40) M28L at a 1.5-fold (gray triangles), or a tenfold molar excess (black triangles). (C) Fractional change in sedimentation coefficient *versus* the concentration of Echistatin variant: rEch (1-49) M28L (filled circles) or rEch (1-40) M28L (gray triangles); the continuous line was determined by fitting to a hyperbolic inhibition model.[10] The open circle denotes the effects of transient exposure to rEch (1-49) M28L.

Effects of recombinant echistatin variants on αIIbβ3 thermal stability

The observation that rEch (1-49) M28L and rEch (1-40) M28L both perturbed αIIbβ3's solution conformation led us to test the hypothesis that the integrin–echistatin complexes would be resistant to thermal aggregation, an effect we have recently described for ligand mimetic peptides.[13] Here we employed dynamic light-scattering measurements as the most direct approach toward determining temperature-induced changes in integrin quaternary structure.

Figure 3(A) depicts the results of particle size measurements performed as a function of temperature with αIIbβ3 alone (open circles) and in the presence of a threefold molar excess rEch (1-49) M28L (filled circles). The ligand-free integrin

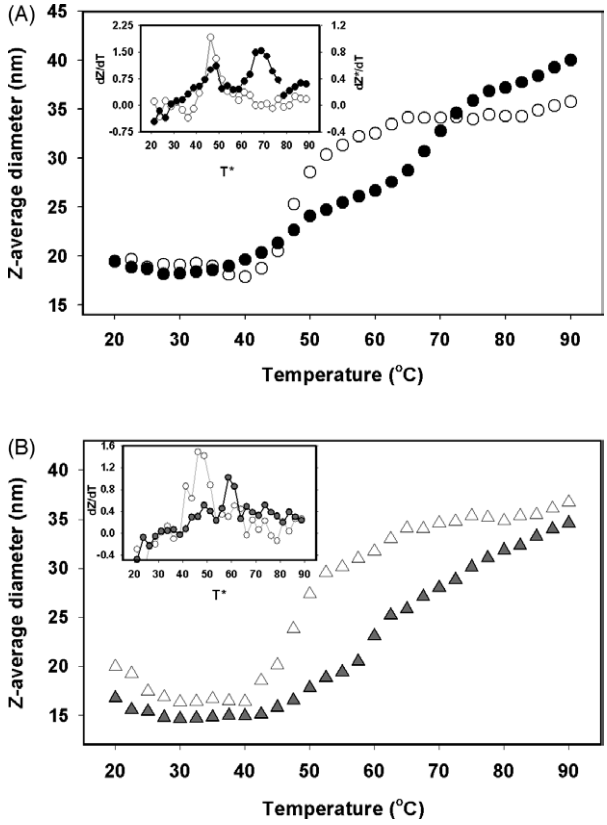

Figure 3. Effects of recombinant echistatin on αIIbβ3 thermal stability determined by dynamic light-scattering. (A) *Z*-average macromolecular diameter measurements performed as a function of temperature are plotted for αIIbβ3 alone (open circles), and +rEch (1-49) M28L at a 3.3-fold molar excess (filled circles). The inset shows the derivative of the *Z*-average diameter with respect to temperature plotted *versus* temperature, d*Z*/d*T*. This procedure enabled the location of a transition mid-point at 46 °C for the free integrin (open circles); the integrin–echistatin complex exhibited a minor peak at 48 °C and a major transition at 69 °C (filled circles). (B) Similar procedures applied in separate experiments to αIIbβ3 alone (open triangles), +rEch (1-40) M28L at a tenfold molar excess (gray triangles) yielded transition mid-points of 46 °C and 59 °C, respectively (inset).

exhibited a sigmoidal increase in particle diameter, increasing from ~19 nm at 20 °C to a plateau at ~35 nm at temperatures above 70 °C. In contrast, the integrin–echistatin complex exhibited a biphasic profile. The transition mid-points were determined by plotting dZ/dT, the incremental change in z-average particle size with temperature, as a function of temperature, as shown in Figure 3(A), inset. This analysis identified a single $T_m = 46$ °C for αIIbβ3 alone. The αIIbβ3: rEch (1–49) M28L sample exhibited two peaks, corresponding to $T_m = 49$ °C and a more pronounced transition at 69 °C. A similar transition at 69 °C was observed in the presence of an 11-fold molar excess of rEch (1–49) M28L (data not shown). In separate experiments, T_m values of 46 °C and 59 °C were obtained for αIIbβ3 alone, and in the presence of a fivefold molar excess of rEch (1-40) M28L (Figure 3(B)), respectively. When present at a 1.4-fold molar excess, rEch (1–40) M28L caused a smaller effect, yielding $T_m =$ 49 °C (data not shown). These data indicate that while echistatin's 11 residue carboxy-terminal segment is not required for the ligand to bind to αIIbβ3, it does contribute to the stabilization of its solution conformation. These observations also provide the first evidence that binding a protein ligand to the αIIbβ3 integrin yields a more thermostable conformer, one similar to that induced by low molecular mass ligands.[13]

Effects of recombinant echistatin variants on αIIbβ3 oligomerization

Since oligomerization or clustering is considered to play a major role in the regulation of integrin function,[51] we tested the hypothesis that integrin: echistatin complexes would exhibit larger self-association constants than the ligand-free receptor. Following procedures optimized with synthetic peptide ligands,[13] we carried out sedimentation equilibrium measurements at temperatures ranging from 20–40 °C, with αIIbβ3 alone, and in the presence of either rEch (1-49) M28L or rEch (1–40) M28L. As illustrated in Figure 4(A), the free integrin (open squares) was stable from 20–35 °C, but it then exhibited a sharp, ~twofold increase in weight-average molecular weight (M_w) at 40 °C. In contrast, the echistatin:integrin complexes (filled circles, rEch (1-49) M28L; filled triangles, rEch (1–40) M28L) each showed substantial, but stable, oligomerization across the temperature range from 20–40 °C. The resultant M_w value ($3.35(\pm 0.16)\times 10^5$) obtained in the presence of rEch (1-49) M28L across this interval was 53% higher than the calculated value for an αIIbβ3 protomer (2.18×10^5); that obtained with rEch (1–40) M28L was 46% greater. These results indicate substantial ligand-induced oligomerization, although even at the highest temperature examined, the observed molecular masses fell between that of an αIIbβ3 protomer and dimer. We have used sedimentation equilibrium measurements to quantify the effects of peptides and pharmaceutical integrin antagonists on αIIbβ3's

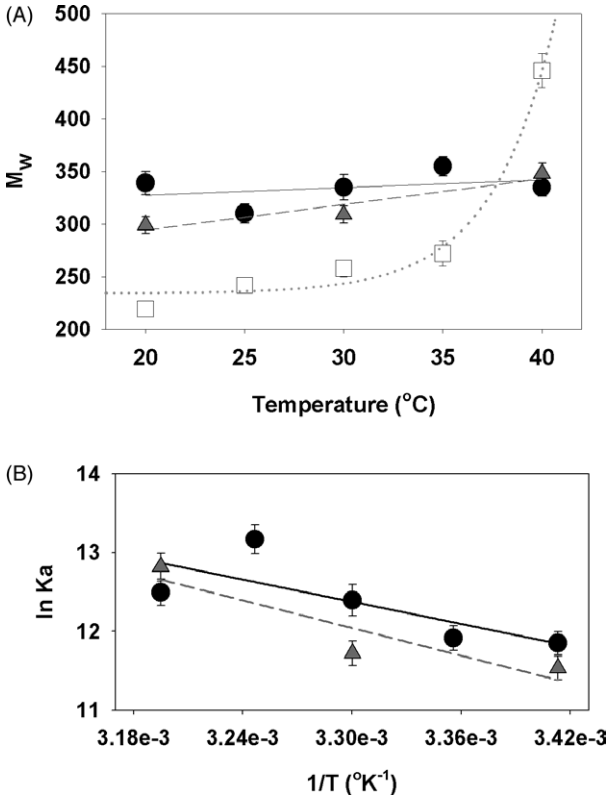

Figure 4. Effects of temperature and recombinant echistatin on αIIbβ3 oligomerization determined by sedimentation equilibrium. (A) Data obtained as a function of temperature for αIIbβ3 alone (open squares), +rEch (1-49) M28L (filled circles), +rEch (1-40) M28L (dark gray triangles) were analyzed with WinNONLIN[53] to obtain weight-average molecular weight values (and their standard deviations) as a function of temperature. (B) Data for the integrin–echistatin complexes in (A) were also analyzed with WinNONLIN to extract dimerization constants; the resultant K_a values (and their standard deviations) are presented in a (linear) van't Hoff plot of $\ln K_a$ *versus* $1/T$ from which thermodynamic parameters were determined.[13]

quaternary structure; however, echistatin's effects on M_w exceed those of any synthetic ligand we have examined.[10–13,52] Since these size distribution data were obtained after the 20 hour period required to achieve sedimentation equilibrium,[10] they report a relatively slow oligomerization process that follows the ligand-induced initial conformational changes detected by sedimentation velocity.

These data were also analyzed with NONLIN[53] to obtain values of K_a, the receptor dimerization constant, as a function of temperature[13] for each integrin–echistatin complex. Addition of higher-order terms to the oligomerization model did not cause a significant improvement in the quality of the fit; therefore, we concluded that a monomer–dimer equilibrium was the simplest model consistent with the data. Consideration of this equilibrium, using our experimentally determined dimerization constants and the range of integrin concentrations

examined, indicates that at 20 °C, 35–45% (by weight) of the integrins will be present as dimers, while at 40 °C, this value will rise to 50–60%. Figure 4(B) depicts the results of van't Hoff analysis, i.e. a plot of ln K_a *versus* $1/T$, from which the following thermodynamic parameters for oligomerization of the integrin: echistatin complexes were determined: $\Delta H = 9.3(\pm 4.5)$ kcal/mol and $\Delta S = 55(\pm 15)$ cal/deg-mol for rEch (1-49 M28L) and $\Delta H = 11.6(\pm 5.0)$ kcal/mol and $\Delta S = 62(\pm 16)$ cal/deg-mol for rEch (1-40 M28L). These data indicate that echistatin's 11 residue carboxy-terminal segment is not required for the ligand to promote αIIbβ3 oligomerization. While the small slope of the van't Hoff plots gives rise to a large uncertainty in the enthalpy data, this pattern of favorable oligomerization entropy partly offset by an unfavorable enthalpy change obtained with the αIIbβ3–echistatin complexes is comparable to the effects of synthetic integrin ligands.[13] Our demonstration that echistatin binding promotes αIIbβ3 oligomerization expands our understanding of the mechanisms that regulate integrin function by demonstrating that a single-domain protein ligand can modulate an integrin's quaternary structure, in a manner similar to that of low molecular mass integrin antagonists.[13,32]

Discussion

This investigation provides insights into the dynamic regulation of integrin function by demonstrating that echistatin binding to the αIIbβ3 integrin stabilizes an open conformer with an enhanced, entropy-driven oligomerization constant. We propose that despite its small size, echistatin can serve as a paradigm for understanding much larger adhesive macromolecules because its ability to modulate αIIbβ3's structure resides on an RGD loop, while full disintegrin activity requires an auxiliary site. Understanding αIIbβ3 integrin structure and function has proven paradoxical because low molecular mass ligand-mimetics (<1500 Da) can readily bind to the resting receptor, yet physiological ligands, such as the 340,000 Da adhesive protein fibrinogen, cannot. By demonstrating that recombinant echistatin can bind to αIIbβ3, isolated without prior exposure to any activating ligands,[11] we have extended the receptors' "size exclusion limit" to at least 6 kDa.

We next turned to the question: what conformational changes are linked to echistatin binding to the resting αIIbβ3 integrin? Hydrodynamic computations[48–50] predict that echistatin binding alone would cause an ~2% increase in αIIbβ3's sedimentation coefficient, whereas ligand-induced asymmetry would decrease the S value from 4–12%. Because our experimental data demonstrate an ~7% decrease in S value for the αIIbβ3:rEch (1–49) M28L complex (Figure 2), we conclude that echistatin binding is linked to a substantial conformational change in αIIbβ3's tertiary structure. Our observation that rEch (1-40) M28L yielded an ~5% decrease in S value indicates that the 11 residues present on echistatin's flexible carboxy terminus[30] are not required for this interaction. It is also likely that the conformational plasticity inherent in integrin structure,[4,5,54–56] a concept reinforced by our electron microscopy observations of a range of integrin sizes and shapes (Figure 1), contributed to the effects of echistatin binding on αIIbβ3's sedimentation profiles.

While we have previously proposed an integrin activation scheme in which ligand mimetic binding is linked to subunit separation in αIIbβ3's head region,[10,12] we now recognize that such a model is incompatible with high resolution structural data that demonstrate short-range electrostatic interactions occur between a cyclic RGD ligand and both subunits in the αvβ3 complex.[6] Hence, we have sought alternative explanations for our observations. For example, If echistatin binding to αIIbβ3's ectodomain were to induce a conformational change that propagates "downward" leading to either release the "deadbolt" proposed to lock an integrin into its bent conformation,[2] or to disrupt interactions between its cytoplasmic domains,[27] the resultant increase in hydrodynamic volume could account for the slower-sedimenting conformers.[57] The magnitude of these echistatin-induced conformational perturbations are comparable to those we have obtained with linear RGDX peptides,[10] but are two- to threefold greater than the effects of tirofiban,[32] a non-peptide integrin antagonist designed to replicate the RGD spatial charge. Tirofiban's smaller size and higher affinity for the αIIbβ3 integrin[32] could explain why its effects on αIIbβ3 conformation were smaller than echistatin's. We may speculate that echistatin operates by an induced fit mechanism,[58] perturbing the receptor's conformation to maximize electrostatic contacts with its target integrin[15,39,40,59] at the expense of binding energy.

We have also demonstrated that echistatin binding is linked to increased integrin oligomerization, as evidenced by sedimentation equilibrium measurements (Figure 4). We may speculate that the conformational perturbation initiated by echistatin binding at the αIIb/β3 subunit interface propagates from the receptor's ectodomain through its stalks, resulting in a disruption of contacts between its distant transmembrane and cytoplasmic regions. In that case, the now unpaired transmembrane segments from two separate integrins could associate to form oligomers. Ligand-induced stalk separation has also been described for the ectodomain of the αvβ3 integrin,[8] and breaking αIIb/β3 transmembrane interactions has been implicated in receptor oligomerization.[44] Furthermore, signaling mechanisms involving activation-induced disruption of cytodomain contacts on the αLβ2 have recently been reported on living cells.[27]

However, one may question whether thermodynamic or kinetic barriers to micelle fusion could hamper transmembrane association in a detergent environment.[60] Resolving this issue experimentally

is not straightforward, as the free energy changes associated with transmembrane helix dimerization in detergent micelles are quite sensitive to the detergent concentration.[61] In fact, Gottschalk *et al*.[60,62] have proposed an alternate integrin activation scheme in which contacts between the αIIb and β3 transmembrane segments are preserved during activation, while a scissors-like movement disrupts interactions between the cytoplasmic domains that stabilize the resting integrin conformation. On the other hand, Weisel and colleagues first observed transmembrane separation with αIIbβ3–fibrinogen complexes,[16] and we subsequently reported the formation of tail-to-tail integrin oligomers in the presence of synthetic ligands.[10,12,13] Recently, Li *et al*.[44] described a similar αIIbβ3 tail separation and oligomerization process induced by divalent manganese cations. While all experiments reported here were carried out in 2 mM $CaCl_2$, we have obtained preliminary data indicating that αIIbβ3 exhibits a similar distribution of sedimenting species and weight-average molecular mass in 2 mM $MnCl_2$. All these studies were performed with integrin receptors solubilized in octyl glucoside micelles. Moreover, proteins have been crystallized in octyl glucoside micelles yielding high resolution structural data for oligomers composed of 2,[63] 6,[64] and 11[65] transmembrane helices. The octyl glucoside molecules typically bound perpendicular to the helix axis, making direct contact with non-polar residues.[63,65] We have incorporated these detergent-binding characteristics into the models we have developed to predict the hydrodynamic parameters of full-length αIIbβ3 integrin protomers and dimers.[13]

The entropy-driven nature of echistatin-induced dimerization supports the concept that interactions between the receptors' hydrophobic transmembrane segments contribute to oligomerization. In fact, the magnitude of the favorable entropy changes, $\Delta S = 55(\pm 15)$ cal/deg-mol determined here for dimerization of the αIIbβ3–rEch (1-49) M28L complex, and $\Delta S = 62(\pm 16)$ cal/deg-mol for rEch (1-40 M28L) are comparable to the parameters we have determined for the pharmaceutical integrin antagonists, tirofiban (66 cal/deg-mol) and eptifibatide (85 cal/deg-mol).[13] Likewise, the integrin dimerization enthalpy changes were all comparably unfavorable for each ligand: rEch (1-49) M28L (9 kcal/mol), rEch (1–40) M28L (12 kcal/mol), tirofiban (13 kcal/mol), eptifibatide (19 kcal/mol).[13] As illustrated in Figure 5, the similar pattern of enthalpy/entropy compensation for protein, ligand-mimetic, and peptide ligands supports that concept that a common ligand-induced oligomerization mechanism is at work. Differences in the magnitude of the initial conformational perturbation may explain the order of effectiveness of these ligands at promoting oligomerization, as evidenced by the magnitude of the following $\Delta G_{dimerization}$ terms: rEch (1–49) M28L (−6.9 kcal/mol) > rEch (1-40) M28L (−6.7 kcal/mol) > eptifibatide (−6.3 kcal/mol) > tirofiban (−6.1 kcal/mol).[13,32]

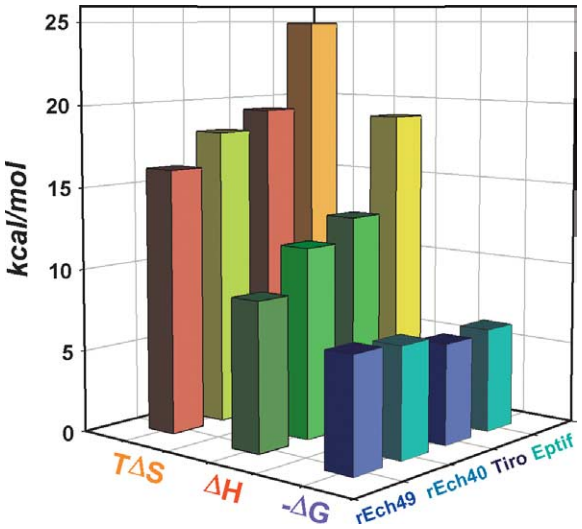

Figure 5. Summary of thermodynamic parameters for ligand-linked integrin oligomerization. The height of each bar denotes the magnitude of the free energy change, $-\Delta G$ (blue/purple color ramp), the enthalpy change, ΔH (green/yellow color ramp), or the temperature-weighted entropy term, $T\Delta S$ (brown/yellow color ramp) for the two echistatin variants examined here, as well as data for the ligand-mimetic tirofiban and thepeptide ligand, eptifibatide, determined in our earlier work.[13,32]

Data obtained in this study support the concept that the ligand-free integrin is more sensitive to thermal aggregation than the receptor–ligand complex. Here we have used dynamic light-scattering to detect increased integrin aggregation with a T_m = 46 °C, comparable to $T_m = 43(\pm 3)$ °C we determined by circular dichroism and intrinsic fluorescence measurements.[13] We have also demonstrated that rEch (1–49) M28L binding protects the αIIbβ3 complex from thermal aggregation, shifting the transition mid-point to 69 °C; the truncation mutant rEch (1–40) M28L was somewhat less effective, yielding a maximum T_m value of 59 °C. These observations extend the concept of ligand-linked thermal protection from synthetic peptides[13] to a protein ligand. While these transitions are clearly outside the physiological temperature range, they do provide additional biophysical evidence that the conformational state of the ligand-occupied integrin differs significantly from its resting counterpart. Others have reported that echistatin binds to resting and activated αIIbβ3 integrins with comparable affinity,[33] yet we have demonstrated that echistatin binding is linked to changes in αIIbβ3's tertiary and quaternary structure. Our observations suggest that echistatin shifts equilibrium amongst resting, activated and clustered integrins toward a thermodynamically stable oligomeric state.

This conformational change issue remains exciting and controversial, as the only available crystallographic data on a β3 integrin show only small ectodomain perturbations between the free and

bound αvβ3 complex.[5,6] In contrast, biophysical probes and electron microscopy have detected rather more substantial changes in tertiary structure for both αIIbβ3 and αvβ3, upon binding synthetic ligands.[8–10,12] Furthermore, SAXS measurements[21] and electron microscopy[26] have yielded somewhat divergent views of the conformational perturbations in α5β1's ectodomain that occur upon binding fibronectin fragments. We anticipate that the lessons learned from echistatin, a model protein ligand, can serve as a paradigm for probing and understanding the structural prerequisites for αIIbβ3's interactions with larger adhesive macromolecules.

Materials and Methods

αIIbβ3 purification

Milligram quantities of highly purified αIIbβ3 were isolated from outdated human blood platelets (American Red Cross, Triad Blood Center, Winston-Salem, NC) as described.[10,11] Biophysical measurements were performed on peak integrin fractions obtained by size exclusion chromatography at 4 °C on a 0.9 cm × 85 cm column of Sephacryl S-300 equilibrated in a pH 7.4 buffer (HSC-OG) containing 0.13 mol/l NaCl, 0.01 mol/l Hepes, 0.002 mol/l $CaCl_2$, 3×10^{-8} mol/l basic trypsin inhibitor, 10^{-6} mol/l leupeptin, 0.02% (w/v) sodium azide, and 0.03 mol/l *n*-octyl-β-D-glucopyranoside. Peak fractions were then concentrated in an Amicon pressure concentrator with a PLHK cellulose membrane, 100,000 Da retention limit.[12] While we do not employ an RGD-affinity column to select for active integrin,[66] we have previously demonstrated that our purified integrin can bind fibrinogen following transient exposure to a ligand-mimetic peptide.[67] Thus our "resting yet responsive" preparation resembles the resting AS1 population described by Yan *et al.*;[66] however, it can be readily activated to the AS2 state.

Cloning, expression, and purification of recombinant echistatin variants

This study employed a plasmid constructed from the vector pGEX-KG, which contains the glutathione-*S*-transferase (GST) gene and a thrombin-sensitive linker.[68] Selected echistatin genes were then inserted at a BamHI restriction site that added four N-terminal amino acid residues (Gly, Ser, Thr, Met) to each disintegrin protein. Vectors expressing full-length echistatin with an M28L mutation, rEch (1–49) M28L, and an inactive truncation variant rEch (1–40) M28L, which is missing the C-terminal sequence Arg-Asn-Pro-His-Lys-Gly-Pro-Ala-Thr, were used here.[38] Plasmid DNA was amplified by transforming *Escherichia coli* strain HB101-1424471, and sequences of the resultant clones were verified (DNA Sequencing Core Laboratory of the Comprehensive Cancer Center of Wake Forest University School of Medicine). rEch (1-49) M28L and rEch (1-40) M28L were expressed in *E. coli* BL21, then isolated from cell lysates by adsorption to glutathione-agarose followed by thrombin-cleavage of the bead-bound constructs.[68]

Each disintegrin was then purified by size-exclusion chromatography on Sephadex G-75 in 0.05 M ammonium acetate buffer (pH 7). Elution was monitored by absorbance at 276 nm; peak fractions were combined, lyophilized and stored at −20 °C. Purity of all recombinant proteins was assessed by SDS-PAGE; concentrations were determined by quantitative amino acid composition analysis.[10] UV–visible spectral measurements performed in a Beckman diode array spectrophotometer with recombinant echistatin samples contained in 1 cm path length/0.1 ml volume quartz cuvettes provided additional characterizations, as each disintegrin construct contains a single tyrosine residue.[38] rEch (1-49) M28L exhibited $\varepsilon_{276}=2300(\pm490)$ l/mol-cm (after correction for turbidity), in agreement with the calculated value of 2030 l/mol-cm. Turbidity problems were more pronounced with rEch (1-40) M28L, which exhibited $\varepsilon_{276}=3120\ (\pm730)$ l/mol-cm.

Mass spectrometry data obtained by MALDI-TOF (performed by the Biomolecular Resource Facility of Wake Forest University) yielded a molecular mass of 5782 Da for rEch (1-49) M28L and 4815 daltons for rEch (1-40) M28L, in reasonable agreement with the calculated average masses of 5775 and 4816 Da for the full-length and truncated disintegrins, respectively (each as fully disulfide-bonded proteins). Mass spectrometry data obtained by ESIMS (Mass Spectrometry Facility of Wake Forest University) yielded a monoisotopic mass of 5773 Da for rEch (1-49) M28L, and peaks at 4816 and 4813 Da for rEch (1-40) M28L. The calculated monoisotopic masses for rEch (1-49) M28L range from 5770.5 (four disulfide bonds) to 5778.5 (eight cysteine residues); for rEch (1-40) M28L, the calculated monoisotopic masses range from 4812–4820 Da.

Platelet function measurements

Platelet-rich plasma (PRP) and gel-filtered platelets (GFP) were isolated from blood obtained by venipuncture from healthy, adult, volunteer donors as described.[69] Platelet counts were determined with a Coulter MDII Cell Counter (Beckman-Coulter, Miami, FL). Platelet aggregation profiles were obtained in a Chrono-Log model 500 aggregometer. Platelet adhesion to fibrin was determined in a mictotiter plate adhesion assay with colorimetric read-out as described.[70] This assay used highly purified human fibrinogen (free of plasminogen and factor XIII), purchased from American Diagnostica (Greenwich, CT), and highly purified human α-thrombin, purchased from Sigma Chemical Co. (St. Louis, MO).

Transmission electron microscopy

αIIbβ3 samples at ∼1 mg/ml in HSC-OG (in the presence/absence of 17 umol/l rEch (1-49 M28L), were incubated for one hour at room temperature, then diluted to ∼20–25 μg/ml in a buffer containing 0.05 mol/l ammonium formate (pH 7.4), 30 mmol/l octyl glucoside, and 15% (v/v) glycerol. Samples were then sprayed onto freshly cleaved mica and shadowed with tungsten in a vacuum evaporator (Denton Vacuum Co., Cherry Hill, NJ).[71–73] These samples were examined in a Philips 400 electron microscope (FEI Co., Hillsboro, OR) operating at 60 kV and a magnification of 60,000×. Size distribution measurements (SigmaScan, Jandel Scientific) were made from prints of the micrographs, using images from many different areas of several different preparations to get a random sample.

Analytical ultracentrifugation measurements

Sedimentation velocity and equilibrium measurements

were performed in a Beckman Optima XL-A analytical ultracentrifuge (Beckman Instruments, Palo Alto, CA) equipped with absorbance optics and an An60 Ti rotor.[10,12] Sedimentation velocity data were collected with the αIIbβ3 complex alone and in the presence of recombinant echistatin variants at 20 °C at a rotor speed of 35,000 rpm. Sedimentation velocity data were analyzed using both SVEDBERG (version 1.04) and DCDT+ (version 6.31) software (J. Philo, Thousand Oaks, CA) to obtain the weight-average sedimentation coefficient (S_w) and distribution of sedimenting species, $g(s^*)$, respectively.[47] All sedimentation coefficients have been corrected for solvent density and viscosity to obtain $s_{20,w}$ values.

The absorbance *versus* radial distance data obtained by sedimentation equilibrium were analyzed by non-linear regression with WinNONLIN3[53] to obtain weight-average molecular weights (M_w) for the αIIbβ3 complex alone and in the presence of rEch (1-49) M28L or rEch (1–40) M28L. These data were collected at temperatures from 20 °C–40 °C at a rotor speed of 7000 rpm. Following procedures previously detailed,[13] data obtained with the integrin:echistatin complexes were subjected to additional analyses with WinNONLIN3 to obtain a set of temperature-dependent self-association constants.[74] WinNONLIN3 was provided by Dr David Yphantis and the staff at the National Analytical Ultracentrifugation Facility, Storrs, CT.

Light-scattering measurements

Static and dynamic light-scattering measurements were performed with the αIIbβ3 complex alone and in the presence of rEch (1-49) M28L or rEch (1–40) M28L in a Malvern Instruments ZEN 1600. Data were collected as a function of temperature from 20 °C −90 °C, in 2.5 deg. C increments; each temperature ramping sequence required ~three hours to complete. The resultant autocorrelation function data were analyzed by the method of cumulants to obtain a *z*-average particle diameter at each temperature. Size distribution information was also obtained from these corrected autocorrelation functions with the CONTIN algorithm.[75]

Computing the hydrodynamic parameters for integrin: echistatin complexes

Models of the αIIbβ3:echistatin complex were obtained by docking an echistatin molecule (2ECH; pdb) to a truncated version of our resting integrin model[13] containing αIIb residues 1–452 and β3 residues 55–432. Following an initial manual alignment†[48] echistatin–integrin contacts were optimized by limited energy minimization using CNS[76]. The resultant echistatin–integrin ectodomain construct was then fused to our full-length models of either the V-shaped,[5] partially bent,[9] extended[13] or "open" integrins.[8] Hydrodynamic parameters for these models were computed with SOMO (SOlution MOdeler) and BEAMS.[48–50]

Acknowledgements

We thank Dr Mark O. Lively, Director of the Biomolecular Resource Facility of Wake Forest University, and Dr Michael J. Thomas, Director of the Mass Spectrometry Facility of Wake Forest University, as well as Mark Morris and Mike Samuel, for mass determinations. We thank Dr Julie Edelson for her expert editorial assistance.

This investigation was supported by Grant-in-Aid 0355869U from the American Heart Association and the Venture Fund of Wake Forest University School of Medicine (to R.R.H.), National Institutes of Health Postdoctoral Fellowship F32-AI051805 (to J.H.C.), National Institutes of Health grant AI15892 (to D.S.L.), European Community grant GI04-CT96-0662 (to M.R.), and National Institutes of Health grant HL 30954 (to J.W.W.).

† The PyMOL Molecular Graphics System DeLano Scientific, San Carlos, CA (2002).

References

1. Hynes, R. O. (2002). Integrins: bidirectional, allosteric signaling machines. *Cell*, **110**, 673–687.
2. Xiong, J. P., Stehle, T., Goodman, S. L. & Arnaout, M. A. (2003). New insights into the structural basis of integrin activation. *Blood*, **102**, 1155–1159.
3. Humphries, M. J., McEwan, P. A., Barton, S. J., Buckley, P. A., Bella, J. & Paul, M. A. (2003). Integrin structure: heady advances in ligand binding, but activation still makes the knees wobble. *Trends Biochem. Sci.* **28**, 313–320.
4. Carman, C. V. & Springer, T. A. (2003). Integrin avidity regulation: are changes in affinity and conformation underemphasized? *Curr. Opin. Cell Biol*, **15**, 547–556.
5. Xiong, J. P., Stehle, T., Diefenbach, B., Zhang, R., Dunker, R., Scott, D. L. *et al*. (2001). Crystal structure of the extracellular segment of integrin αVβ3. *Science*, **294**, 339–345.
6. Xiong, J. P., Stehle, T., Zhang, R., Joachimiak, A., Frech, M., Goodman, S. L. & Arnaout, M. A. (2002). Crystal structure of the extracellular segment of integrin αVβ3 in complex with an Arg-Gly-Asp ligand. *Science*, **296**, 151–155.
7. Weisel, J. W., Nagaswami, C., Vilaire, G. & Bennett, J. S. (1992). Examination of the platelet membrane glycoprotein IIb–IIIa complex and its interaction with fibrinogen and other ligands by electron microscopy. *J. Biol. Chem.* **267**, 16637–16643.
8. Takagi, J., Petre, B. M., Walz, T. & Springer, T. A. (2002). Global conformational rearrangements in integrin extracellular domains in outside–in and inside–out signaling. *Cell*, **110**, 599–611.
9. Adair, B. D. & Yeager, M. (2002). Three-dimensional model of the human platelet integrin αIIbβ3 based on electron cryomicroscopy and X-ray crystallography. *Proc. Natl Acad. Sci. USA*, **99**, 14059–14064.
10. Hantgan, R. R., Paumi, C., Rocco, M. & Weisel, J. W. (1999). Effects of ligand-mimetic peptides Arg-Gly-Asp-X (X=Phe, Trp, Ser) on αIIbβ3 integrin conformation and oligomerization. *Biochemistry*, **38**, 14461–14464.
11. Hantgan, R. R., Braaten, J. V. & Rocco, M. (1993). Dynamic light scattering studies of $\alpha_{IIb}\beta_3$ solution conformation. *Biochemistry*, **32**, 3935–3941.
12. Hantgan, R. R., Rocco, M., Nagaswami, C. & Weisel, J. W. (2001). Binding of a fibrinogen mimetic stabilizes integrin αIIbβ3's open conformation. *Protein Sci.* **10**, 1614–1626.
13. Hantgan, R. R., Lyles, D. S., Mallett, T. C., Rocco, M.,

Nagaswami, C. & Weisel, J. W. (2003). Ligand binding promotes the entropy-driven oligomerization of integrin αIIbβ3. *J. Biol. Chem.* **278**, 3417–3426.
14. Liddington, R. C. (2002). Will the real integrin please stand up? *Structure*, **10**, 605–607.
15. Arnaout, M. A., Goodman, S. L. & Xiong, J.-P. (2002). Coming to grips with integrin binding to ligands. *Curr. Opin. Cell Biol.* **14**, 641–651.
16. Weisel, J. W., Nagaswami, C., Vilaire, G. & Bennett, J. S. (1992). Examination of the platelet membrane glycoprotein IIb–IIIa complex and its interaction with fibrinogen and other ligands by electron microscopy. *J. Biol. Chem.* **267**, 16637–16643.
17. Nermut, M. V., Green, N. M., Eason, P., Yamada, S. S. & Yamada, K. M. (1988). Electron microscopy and structural model of human fibronectin receptor. *EMBO J.* **7**, 4093–4099.
18. Carrell, N. A., Fitzgerald, L. A., Steiner, B., Erickson, H. P. & Phillips, D. R. (1985). Structure of human platelet glycoproteins IIb and IIIa as determined by electron microscopy. *J. Biol. Chem.* **260**, 1743–1749.
19. Xiong, J. P., Stehle, T., Goodman, S. L. & Arnaout, M. A. (2003). Integrins, cations and ligands: making the connection. *J. Thromb. Haemost.* **1**, 1642–1654.
20. Liddington, R. C. & Ginsberg, M. H. (2002). Integrin activation takes shape. *J. Cell Biol.* **158**, 833–839.
21. Mould, A. P., Symonds, E. J., Buckley, P. A., Grossmann, J. G., McEwan, P. A., Barton, S. J. *et al.* (2003). Structure of an integrin-ligand complex deduced from solution X-ray scattering and site-directed mutagenesis. *J. Biol. Chem.* **278**, 39993–39999.
22. Takagi, J. & Springer, T. A. (2002). Integrin activation and structural rearrangement. *Immunol. Rev.* **186**, 141–163.
23. Beglova, N., Blacklow, S. C., Takagi, J., Springer, T. A. (2002). Cysteine-rich module structure reveals a fulcrum for integrin rearrangement upon activation. *Nature Struct. Biol.* **9**, 282–287.
24. Luo, B. H., Springer, T. A. & Takagi, J. (2003). Stabilizing the open conformation of the integrin headpiece with a glycan wedge increases affinity for ligand. *Proc. Natl Acad. Sci. USA*, **100**, 2403–2408.
25. Luo, B. H., Springer, T. A. & Takagi, J. (2003). High affinity ligand binding by integrins does not involve head separation. *J. Biol. Chem.* **278**, 17185–17189.
26. Takagi, J., Strokovich, K., Springer, T. A. & Walz, T. (2003). Structure of integrin α5β1 in complex with fibronectin. *EMBO J.* **22**, 4607–4615.
27. Kim, M., Carman, C. V. & Springer, T. A. (2003). Bidirectional transmembrane signaling by cytoplasmic domain separation in integrins. *Science*, **301**, 1720–1725.
28. Gan, Z. R., Gould, R. J., Jacobs, J. W., Friedman, P. A. & Polokoff, M. A. (1988). Echistatin. A potent platelet aggregation inhibitor from the venom of the viper, *Echis carinatus*. *J. Biol. Chem.* **263**, 19827–19832.
29. Saudek, V., Atkinson, R. A. & Pelton, J. T. (1991). Three-dimensional structure of echistatin, the smallest active RGD protein. *Biochemistry*, **30**, 7369–7372.
30. Atkinson, R. A., Saudek, V. & Pelton, J. T. (1994). Echistatin: the refined structure of a disintegrin in solution by ^{1}H NMR and restrained molecular dynamics. *Int. J. Pept. Protein Res.* **43**, 563–572.
31. Chen, Y., Suri, A. K., Kominos, D., Sanyal, G., Naylor, A. M., Pitzenberger, S. M. *et al.* (1994). Three-dimensional structure of echistatin and dynamics of the active site. *J. Biomol. NMR*, **4**, 307–324.
32. Hantgan, R. R., Stahle, M. C., Jerome, W. G., Nagaswami, C. & Weisel, J. W. (2002). Tirofiban blocks platelet adhesion to fibrin with minimal perturbatin of GpIIb/IIIa structure. *Thromb. Haemost.* **87**, 910–917.
33. Bednar, R. A., Gaul, S. L., Hamill, T. G., Egbertson, M. S., Shafer, J. A., Hartman, G. D. *et al.* (1998). Identification of low molecular weight gp iib/iiia antagonists that bind preferentially to activated platelets. *J. Pharmacol. Expt. Ther.* **285**, 1317–1326.
34. Shattil, S. J. (1999). Signaling through platelet integrin αIIbβ3: inside–out, outside–in, and sideways. *Thromb. Haemost.* **82**, 318–325.
35. Tomiyama, Y., Tsubakio, T., Piotrowicz, R. S., Kurata, Y., Loftus, J. C. & Kunicki, T. J. (1992). The Arg-Gly-Asp (RGD) recognition site of platelet glycoprotein IIb–IIIa on nonactivated platelets is accessible to high-affinity macromolecules. *Blood*, **79**, 2303–2312.
36. D'Souza, S. E., Ginsberg, M. H. & Plow, E. F. (1991). Arginyl-glycyl-aspartic acid (RGD): a cell adhesion motif. *Trends Biochem. Sci.* **16**, 246–250.
37. Marcinkiewicz, C., Vijay-Kumar, S., McLane, M. A. & Niewiarowski, S. (1997). Significance of RGD loop and C-terminal domain of echistatin for recognition of αIIbβ3 and αvβ3 integrins and expression of ligand-induced binding site. *Blood*, **90**, 1565–1575.
38. Wierzbicka-Patynowski, I., Niewiarowski, S., Marcinkiewicz, C., Calvete, J. J., Marcinkiewicz, M. M. & McLane, M. A. (1999). Structural requirements of echistatin for the recognition of αVβ3 and α5β1 integrins. *J. Biol. Chem.* **274**, 37809–37814.
39. Scheibler, L., Mierke, D. F., Bitan, G., Rosenblatt, M. & Chorev, M. (2001). Identification of a contact domain between echistatin and the integrin αVβ3 by photo-affinity cross-linking. *Biochemistry*, **40**, 15117–15126.
40. Yahalom, D., Wittelsberger, A., Mierke, D. F., Rosenblatt, M., Alexander, J. M. & Chorev, M. (2002). Identification of the principal binding site for RGD-containing ligands in the αVβ3 integrin: a photoaffinity cross-linking study. *Biochemistry*, **41**, 8321–8331.
41. Shimaoka, M., Lu, C., Salas, A., Xiao, T., Takagi, J. & Springer, T. A. (2002). Stabilizing the integrin alpha M inserted domain in alternative conformations with a range of engineered disulfide bonds. *Proc. Natl Acad. Sci. USA*, **99**, 16737–16741.
42. Hantgan, R. R. (1988). Fibrin protofibril and fibrinogen binding to ADP-stimulated platelets: evidence for a common mechanism. *Biochim. Biophys. Acta*, **968**, 24–35.
43. Hantgan, R. R., Taylor, R. G. & Lewis, J. C. (1985). Platelets interact with fibrin only after activation. *Blood*, **65**, 1299–1311.
44. Li, R., Mitra, N., Gratkowski, H., Vilaire, G., Litvinov, R., Nagasami, C., Weisel, J. W. *et al.* (2003). Activation of integrin αIIbβ3 by modulation of transmembrane helix associations. *Science*, **300**, 795–798.
45. Edwards, A. L. (1979). *Multiple Regression and the Analysis of Variance and Covariance*. W. H. Freeman and Company, San Francisco pp. 1–212.
46. Koradi, R., Billeter, M. & Wuthrich, K. (1996). MOLMOL: a program for display and analysis of macromolecular structures. *J. Mol. Graph.* **14**, 51–55.
47. Stafford, W. F., III (1992). Boundary analysis in sedimentation transport experiments: a procedure for obtaining sedimentation coefficient distributions using the time derivative of the concentration profile. *Anal. Biochem.* **203**, 295–301.
48. Spotorno, B., Piccinini, L., Tassara, G., Ruggiero, C., Nardini, M., Molina, F. & Rocco, M. (1997). BEAMS (beads modeling system): a set of computer programs

for the visualization and the computation of hydrodynamic and conformational properties of beads models of proteins. *Eur. Biophys. J.* **25**, 373–384.
49. Ray, N. (2001). The development of experimental and computational tools for studying protein interactions: applied to the bacterial toxin pneumolysin. PhD Thesis, University of Glasgow, UK.
50. Byron, O. (2000). Hydrodynamic bead modeling of biological macromolecules. *Methods Enzymol.* **321**, 278–304.
51. Buensuceso, C., De Virgilio, M. & Shattil, S. J. (2003). Detection of integrin αIIbβ3 clustering in living cells. *J. Biol. Chem.* **278**, 15217–15224.
52. Hantgan, R. R., Lyles, D. S., Rocco, M. & Weisel, J. W. (2002). Ligation effects the thermal stability of integrin αIIbβ3. *Biophys. J.* **82**, 38.
53. Johnson, M., Correia, J. J., Yphantis, D. A. & Halvorson, H. (1981). Analysis of data from the analytical ultracentrifuge by nonlinear least-square techniques. *Biophys. J.* **36**, 575–588.
54. Arnaout, M. A. (2002). Integrin structure: new twists and turns in dynamic cell adhesion. *Immunol. Rev.* **186**, 125–140.
55. Shimaoka, M., Takagi, J. & Springer, T. A. (1931). Conformational regulation of integrin structure and function. *Annu. Rev. Biophys. Biomol. Struct.* **2002**, 485–516.
56. Rivas, G. A., Aznarez, J. A., Usobiaga, P., Salz, J. L. & Gonzalez-Rodriguez, J. (1991). Molecular characterization of the human platelet integrin gpIIb/IIIa and its constituent glycoproteins. *Eur. Biophys. J.* **19**, 335–345.
57. Rocco, M., Spotorno, B. & Hantgan, R. R. (1993). Modeling the αIIbβ3 integrin solution conformation. *Protein Sci.* **2**, 2154–2166.
58. Creigton, T. E. (1993). Enzyme catalysis. In *Proteins: Structures and Molecular Properties* (Creigton, T. E., ed), pp. 385–461, W. H. Freeman and Company, New York.
59. Feuston, B. P., Culberson, J. C., Duggan, M. E., Hartman, G. D., Leu, C. T. & Rodan, S. B. (2002). Binding model for nonpeptide antagonists of αVβ3 integrin. *J. Med. Chem.* **45**, 5640–5648.
60. Gottschalk, K. E., Adams, P. D., Brunger, A. T. & Kessler, H. (2002). Transmembrane signal transduction of the αIIbβ3 integrin. *Protein Sci.* **11**, 1800–1812.
61. Fleming, K. G. (2002). Standardizing the free energy change of transmembrane helix-helix interactions. *J. Mol. Biol.* **323**, 563–571.
62. Gottschalk, K. E. & Kessler, H. (2004). Evidence for hetero-association of transmembrane helices of integrins. *FEBS Letters*, **557**, 253–258.
63. Kumar, M. S., Carson, M., Hussain, M. M. & Murthy, H. M. (2002). Structures of apolipoprotein A-II and a lipid-surrogate complex provide insights into apolipoprotein–lipid interactions. *Biochemistry,* **41**, 11681–11691.
64. Shu, W., Ji, H. & Lu, M. (2000). Interactions between HIV-1 gp41 core and detergents and their implications for membrane fusion. *J. Biol. Chem.* **275**, 1839–1845.
65. Roth, M., Ducruix, A. & Husson-Reiss, F. (1991). Structure of the detergent phase and protein-detergent interactions in crystals of the wild-type (Strain Y) *Rhodobacter sphaeroides* photochemical reaction center. *Biochemistry,* **30**, 9403–9413.
66. Yan, B., Hu, D. D., Knowles, S. K. & Smith, J. W. (2000). Probing chemical and conformational differences in the resting and active conformers of platelet integrin αIIbβ3. *J. Biol. Chem.* **275**, 7249–7260.
67. Bonnefoy, A., Hantgan, R., Legrand, C. & Frojmovic, M. M. (2001). A model of platelet aggregation involving multiple interactions of thrombospondin-1, fibrinogen, and GPIIbIIIa receptor. *J. Biol. Chem.* **276**, 5605–5612.
68. Smith, D. B. & Johnson, K. S. (1988). Single-step purification of polypeptides expressed in *Escherichia coli* as fusions with glutathione S-transferase. *Gene*, **67**, 31–40.
69. Hantgan, R. R. (1984). A study of the kinetics of ADP-triggered platelet shape change. *Blood*, **64**, 896–906.
70. Hantgan, R. R., Stahle, M., Del, G. V., Adams, M., Lasher, T., Jerome, W. G. *et al*. (2001). αIIb's cytoplasmic domain is not required for ligand-induced clustering of integrin αIIbβ3. *Biochim. Biophys. Acta*, **1540**, 82–95.
71. Fowler, W. E. & Erickson, H. P. (1979). Trinodular structure of fibrinogen. Confirmation by both shadowing and negative stain electron microscopy. *J. Mol. Biol.* **134**, 241–249.
72. Veklich, Y. I., Gorkun, O. V., Medved, L. V., Nieuwenhuizen, W. & Weisel, J. W. (1993). Carboxyl-terminal portions of the α chains of fibrinogen and fibrin. Localization by electron microscopy and the effects of isolated αC fragments on polymerization. *J. Biol. Chem.* **268**, 13577–13585.
73. Weisel, J. W., Stauffacher, C. V., Bullitt, E. & Cohen, C. (1985). A model for fibrinogen: domains and sequence. *Science*, **230**, 1388–1391.
74. Laue, T. M. (1995). Sedimentation equilibrium as a thermodyamic tool. *Methods Enzymol.* **259**, 427–452.
75. Provencher, S. W. (1982). CONTIN: a general purpose constrained regularization program for inverting noisy linear algebraic and integral equations. *Comp. Phys. Commun.* **27**, 229–242.
76. Brunger, A. T., Adams, P. D., Clore, G. M., DeLano, W. L., Gros, P., Grosse-Kunstleve, R. W. *et al*. (1998). Crystallography & NMR system: a new software suite for macromolecular structure determination. *Acta Crystallog. sect. D*, **54**, 905–921.
77. Philo, J. S. (1997). An improved function for fitting sedimentation velocity data for low-molecular-weight solutes. *Biophys. J.* **72**, 435–444.

Edited by W. Baumeister

(Received 4 June 2004; received in revised form 3 August 2004; accepted 4 August 2004)